An Optimal Control Model for Determining Articular Contact Forces at the Human Knee During Rising from a Static Squat Position

Seonpil Kim* and Marcus G. Pandy**

(*Received November 24, 1997*)

A two-dimensional dynamic model of the knee joint was incorporated into a four-segment, eight-muscle model of the human body to determine the muscle, ligament, and articular contact forces transmitted at the knee as humans stand up from a static squatting position. Our optimal control model predicted peak tibiofemoral contact forces 8 times as high as body weight. Furthermore, ligament forces, especially those in the anterior-cruciate, were nearly body weight as knee flexion approached 90 degrees. Ligament and tibiofemoral contact loads were dominated by the forces exerted by muscles during the movement.

Key Words: Knee Modeling, Optimal Control, Musculoskeletal Dynamics

1. Introduction

The knee is the largest and one of the most complex joints in the body. The intricate arrangement of articulating bones, constraining ligaments, and actuating muscles provides for a substantial range of flexibility and loading patterns. However, the knee is also one of the most frequently injured and surgically repaired joints in the body. One of the most common types of knee injuries involves failure of the ligamentous structures which provide stability of the tibia on the femur. Failure of these structures is thought to be partially compensated for by changes in muscular coordination during locomotor activities. However, if left uncorrected subsequent damage is likely to occur in the articulating surfaces and soft tissues in and around the joint.

Knowledge of the forces transmitted by muscles, ligaments, and the articular surfaces at the knee is fundamental for understanding the mechanics of the normal knee and for improving the diagnosis of patients with movement disabilities resulting from knee injury. Unfortunately, muscle, ligament, and joint contact forces cannot be measured non-invasively. Furthermore, because the ligaments and number of muscles form a structurally indeterminate system, straightforward methods employing force and moment equilibrium cannot be used to determine the forces in these structures. A potentially powerful method for determining muscle forces during movement is the combination of musculoskeletal modeling and optimal control theory. The power of an optimal control approach derives from the scope of the modeling: not only does optimal control theory take into account musculotendon dynamics (i. e., muscle's force-length-velocity-activation property), but it also delivers a purely predictive result independent of experiment.

Though numerous attempts have been made to develop two- and three-dimensional models of the human knee joint (Andriacchi et al., 1983; Blankevoort, 1991; Cheng, 1988; Collins and O' Connor, 1991; Fijan, 1990; Morrison, 1970; Wismans et al., 1980; Yamaguchi and Zajac, 1989), no one has combined a dynamical model of the knee with an optimal control approach to determine the forces transmitted at the knee dur-

* Technical Center Samsung Motors Inc. Yongin-city, Kyungki-do, Korea

** Mechanical Engineering University of Texas at Austin Austin, Texas 78712, U. S. A.

ing movement. Abdel-Rahman and Hefzy (1993), Moeinzadeh et al. (1983), and Wong chaisuwat et al. (1984) have developed two-dimensional dynamical models of the knee joint, but all of these neglect the effects of musculotendon dynamics. Andriacchi et al. (1983), Blankevoort (1991), Fijan (1990), and Wismans et al. (1980) have developed more complex three-dimensional models of the knee, but these are either static or quasi-static, and they all neglect the effects of muscle dynamics.

We have developed a two-dimensional dynamical model of the human knee joint to study the mechanics of the normal knee during movement. The knee is represented as a two degree-of-freedom planar joint, which includes the interactions of the femur, tibia, patella, and ligaments. By incorporating the planar knee model into an existing musculoskeletal model of the human body, we then used optimal control theory to determine the muscle, ligament, and articular contact forces transmitted at the knee as humans stand up from a static squatting position.

2. Planar Knee Model

We modeled the knee as a planar joint comprising the tibia, femur, patella, and ligaments (see Fig. 1). Elliptical curves were used to represent the shape of the distal femur in the sagittal plane. A straight line sloping 8 degrees below the normal to the tibial axis was used to represent the weight-bearing surface of the tibial plateau (Nisell, 1985; Yamaguchi and Zajac, 1989). For motion in the sagittal plane, the patella was represented as a rectangle. To model the patella as a spacer and a lever, we assumed that a single point of contact exists between the femoral condyles and the rectangular patella, and that the length of the patella ligament remains constant (Yamaguchi and Zajac, 1989). Because the mass of the patella is small in comparison with that of the femur and tibia, we assumed the patella to be massless so that its motion can be determined purely from the conditions of static equilibrium (see below). Also, since we are interested in normal knee mechanics as it relates to whole-body movement, we neglected the effects of articular cartilage and the menisci.

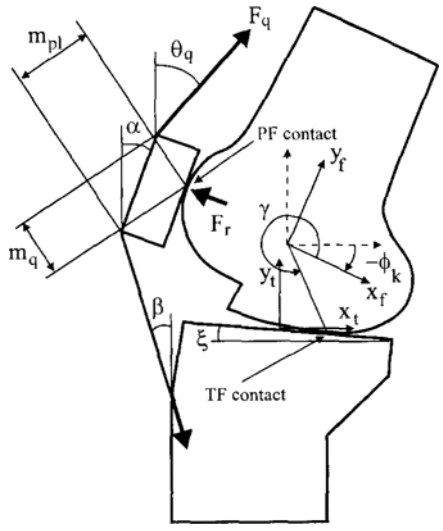

Fig. 1 Schematic of the two-dimensional model of the human knee joint. Elliptical curves were used to represent the shapes of the femoral condyles in the sagittal plane. A straight line with slope $\xi=8°$ was used to represent the weight-bearing surface of the tibial plateau. The patella was represented as a rectangle. α is the orientation of the patella with respect to the vertical, β is the orientation of the patellar ligament with respect to the vertical, F_q and θ_q are the magnitude and direction of the applied quadriceps force, x_k, y_k, and θ_k are the generalized coordinates defining the position of the femur relative to the tibia, (x_f, y_f) represents the reference frame attached to the femur, (x_t, y_t) represents the tibial reference frame, F_r is the patellofemoral force, r and γ define the location of the tibiofemoral contact point with respect to the tibial reference frame, and m_{pl} and m_q are the moment arms of the patellar tendon and the quadriceps, respectively.

2.1 Ligament properties

We included the action of the anterior and posterior-cruciate ligaments and the medial and lateral-collateral ligaments in the planar knee model. The origin and insertion sites of each ligament were obtained from data reported by Garg (1990) and Moeinzadeh et al. (1983). Each

ligament was modeled as a separate bundle of fibers, and its mechanical behavior was described by a nonlinear stress-strain curve (Blankevoort, 1991). Since no experimental data exist for ligament slack lengths, we placed the knee in full extension and adjusted slack lengths until the strain in the anterior- cruciate and lateral-collateral ligaments was 5 percent, and that in the posterior-cruciate and medial-collateral ligament was -1 percent and 5 percent, respectively (Wismans et al., 1980).

2.2 Tibiofemoral joint

We modeled planar motion of the knee using three generalized coordinates to describe flexion-extension, anterior-posterior translation, and compression-distraction of the femur relative to the tibia. Therefore, the unconstrained, planar model has 3 degrees of freedom described by the coordinates x_k, y_k, and ϕ_k (Fig. 1). If the femur slips and rotates on the tibia, only one holonomic constraint is needed to specify knee motion. This kinematical constraint equation can be derived from the following two conditions: i) a geometric compatibility condition which requires that the femoral condyles remain in contact with the tibial plateau during flexion-extension of the knee, and ii) a surface contact condition which necessitates that the femur and tibia do not penetrate each other. Thus, only two independent coordinates are needed to describe motion of the femur relative to the tibia.

To derive the equations representing the compatibility condition, the coordinates of

the tibiofemoral contact point (x_p, y_p) must first be expressed in the femoral and tibial

reference frames (see Fig. 1). Thus,

$$\begin{pmatrix} x_p \\ y_p \end{pmatrix}_{\text{femur}} = \begin{pmatrix} a\cos\gamma \\ b\sin\gamma \end{pmatrix}_{\text{femur}} \tag{1}$$

and

$$\begin{pmatrix} x_p \\ y_p \end{pmatrix}_{\text{tibia}} = \begin{pmatrix} r\cos\xi \\ -r\sin\xi \end{pmatrix}_{\text{tibia}} \tag{2}$$

where a and b are parameters representing the surface shape of the femoral condyles (i. e., the lengths of the major and minor axes of an ellipse), ξ is the angle of inclination of the tibial plateau with respect to the horizontal ($\xi=8°$ Fig. 1), γ is the angle to represent the tibiofemoral contact point, and r is the distance from the origin of the tibial reference frame to the tibiofemoral contact point (Fig. 1). Note that g is not the angle of the vector drawn from the origin of the femoral reference frame to the tibiofemoral contact point.

The contact point of the femur on the tibia, written in terms of the 3 generalized coordinates (x_k, y_k, f_k) can be expressed as

$$\begin{pmatrix} x_p \\ y_p \end{pmatrix}_{\text{tibia}} = \begin{pmatrix} \cos\phi_k & -\sin\phi_k \\ \sin\phi_k & \cos\phi_k \end{pmatrix} \begin{pmatrix} a\cos\gamma \\ b\sin\gamma \end{pmatrix}_{\text{femur}} + \begin{pmatrix} x_k \\ y_k \end{pmatrix} \tag{3}$$

The surface contact condition is obtained by requiring the tangent vectors to the femur and tibia at the tibiofemoral contact point to remain collinear during knee flexion-extension. Expressing the tangent vector at the point of contact between the femur and tibia in the femoral and tibial reference frames,

$$\underline{g}_f = \begin{pmatrix} a\sin\gamma \\ b\cos\gamma \end{pmatrix}_{\text{femur}} \tag{4}$$

and

$$\underline{g}_t = \begin{pmatrix} 1 \\ -\tan\xi \end{pmatrix}_{\text{tibia}} \tag{5}$$

the surface contact condition is found from

$$\underline{g}_t \times \left(\underline{g}_f\right)_{\text{tibia}} = \underline{0} \tag{6}$$

where the tangent vector of the point of contact on the femur is expressed in the tibial reference frame. Referring to Fig. 1, Eq. (6) can be written explicitly as

$$a\sin\gamma(-\cos\phi_k\sin\xi - \sin\phi_k\cos\xi) + b\cos\gamma(-\sin\phi_k\sin\xi + \cos\phi_k\cos\xi) = 0 \tag{7}$$

Also, using Eqs. (2) and (3), the coordinates of the contact point between the femur and tibia can be written as

$$\begin{pmatrix} x_k \\ y_k \end{pmatrix} = \begin{pmatrix} r\cos\xi - (a\cos\gamma\cos\phi_k - b\sin\gamma\sin\phi_k) \\ -r\sin\xi - (a\cos\gamma\sin\phi_k + b\sin\gamma\cos\phi_k) \end{pmatrix} \tag{8}$$

Equations (7) and (8) are the geometric compatibility and surface contact conditions for motion of the femur on the tibia. Since the femur is assumed to rotate and slip on the tibia, our two-dimensional model of the knee requires one holonomic constraint. The holonomic constraint equation can be derived by differentiating Eqs. (7) and (8) with respect to time. Thus,

$$u_1\dot{\gamma}+u_2\dot{\phi}_k=0 \tag{9}$$

$$\dot{x}_k=v_{11}\dot{r}+v_{21}\dot{\gamma}+v_{31}\dot{\phi}_k \tag{10}$$

and

$$\dot{y}_k=v_{12}\dot{r}+v_{22}\dot{\gamma}+v_{32}\dot{\phi}_k \tag{11}$$

Solving Eqs. (9)-(11) for and allows these variables to be eliminated from the above equations so that one holonomic constraint remains. Thus,

$$g_1\dot{x}_k+\dot{y}_k+g_2\dot{\phi}_k=0 \tag{12}$$

where g_1 and g_2 are functions of the location of the tibiofemoral contact point (r and γ) and of the three generalized coordinates defining the position and orientation of the femur relative to the tibia (x_k, y_k, ϕ_k). Given the location of the tibiofemoral contact point and knee flexion angle, the variables r, γ, x_k and yk can all be found using Eqs. (7) and (8).

2.3 Patellofemoral joint

To model the patella as a spacer and a lever, we assumed that a single point of contact exists between the femur and the patella. The patella was represented as a rectangle with length 3.94 cm and thickness 1.63 cm (Yamaguchi and Zajac, 1989). Both the patella and the patellar ligament are assumed to be rigid and inextensible. In particular, if the length of the patella ligament is assumed to remain constant, then the parameters which define the geometry of the patellofemoral joint (a and b) can be calculated given the location of the tibiofemoral contact point and the angle of knee flexion (see Yamaguchi and Zajac, 1989 for details).

Under the assumptions that the patella is massless, that the length of the patellar ligament is constant, and that friction between the patella and femur is negligible, the conditions for static equilibrium completely define the position of the patella for any given angle of knee flexion. Summing the forces acting on the patella gives (see Fig. 1):

$$\begin{pmatrix}-\cos\alpha\\ \sin\alpha\end{pmatrix}F_r+\begin{pmatrix}\sin\beta\\ -\cos\beta\end{pmatrix}Fp_1+\begin{pmatrix}\sin\theta_q\\ \cos\theta_q\end{pmatrix}F_q=\underline{0} \tag{13}$$

and summing moments about the patellofemoral contact point yields

$$m_{p1}F_{p1}=m_qF_q \tag{14}$$

where F_q is the applied force in the quadriceps, F_r is the force exerted on the patella at the patellofemoral joint, F_{p1} is the applied force in the patellar ligament, and m_{p1} and m_q are the perpendicular distances from the line of action of the patellar ligament force and the quadriceps force to the patellofemoral contact point, respectively (Fig. 1). Note that α, β, θ_q, and m_{p1} in Eqs. (13)-(14) are all dependent.

Substituting Eq. (14) into Eq. (13) gives one constraint equation which defines the position of the patella:

$$-m_q\cos(\alpha+\beta)+m_{p1}\cos(\alpha-\theta_q)=0 \tag{15}$$

All of the variables in Eq. (15) can be found by knowing the geometry of the patellofemoral joint. Specifically, we specified the position of the patella by solving a static optimization problem to determine the values of all the muscle forces and the location of the tibiofemoral contact force. Knowing the location of the tibiofemoral contact force, we then solved equation (15) iteratively to obtain values for a and b which specify the orientation of the patella and the patellar ligament, respectively (Fig. 1). Eq. (15) was solved by guessing a value for a and computing the values of all the other variables until both sides of the equation were satisfied identically. Finally, the patellar ligament force and the patellofemoral contact force were computed from

$$F_{p_1}=\frac{m_q}{m_{p1}}F_q \tag{16}$$

and

$$F_r=\frac{\sin(\theta_q+\beta)}{\cos(\alpha+\beta)}F_q \tag{17}$$

3. Musculoskeletal Model of the Human Body

We modeled the human body as a four-segment, articulated, planar linkage actuated by eight muscles (Fig. 2). The metatarsals, ankle, and hip were all modeled as frictionless revolute joints, while the knee was represented as a three degree-of-freedom, planar joint with one holonomic constraint (Fig. 1). Each muscle was modeled as a three-element, lumped-parameter entity in series with tendon. The mechanical behavior of muscle was described by a Hill-type contractile element which modeled its force-length-velocity-activation property, a series-elastic element which modeled its active stiffness, and a parallel-elastic element which modeled its passive stiffness. Tendon was assumed to be elastic, and its properties were modeled by a linear stress-strain curve. The details of our musculotendon model are given in (Pandy et al., 1990).

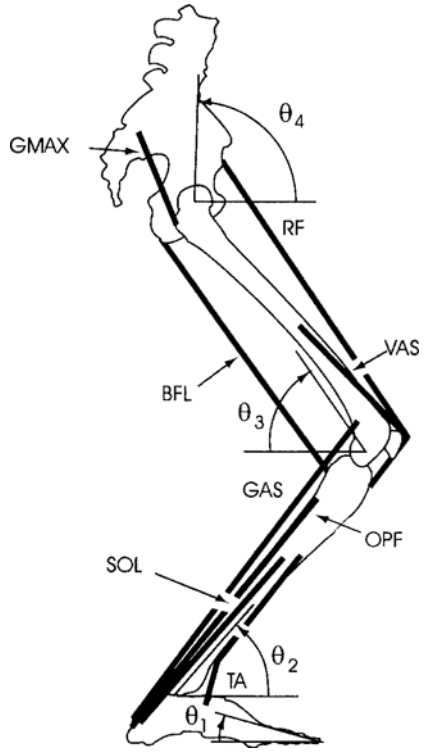

Fig. 2 Schematic of the musculoskeletal model used to simulate rising from a static squatting position. The human body was modeled as a four-segment, planar linkage, actuated by eight musculotendinous units. Symbols appearing in the diagram are: tibialis anterior (TA), soleus (SOL), other uniarticular plantar flexors (OPF), gastrocnemius (GAS), vasti (VAS), rectus femoris (RF), hamstrings (HAMS), and gluteus maximus (GMAX).

3.1 Musculotendinoskeletal dynamics

The dynamical equations of motion for the musculotendinoskeletal system can be written as:

$$A(q)\,\underline{\ddot{q}} - Q(q)^T\underline{\lambda} = [B(q)\,\underline{\dot{q}}^2 + C(q) + DM(q)\,\underline{F}^{MT} + S(q,\ \dot{q})] \tag{18}$$

$$Q(q)\,\underline{\dot{q}} = 0 \tag{19}$$

$$\dot{F}_i^{MT} = f_i(q,\ \dot{q},\ F^{MT},\ a_i);\ i = 1,\ 8 \tag{20}$$

$$\dot{a}_i = (1/\tau_{\text{rise}})\,(u_i - a_i)\,u_i + (1/\tau_{\text{fall}})\,[u_i - (a_i - a_{\min}) - (u_i - a_i)\,u_i];\ i = 1,\ 8 \tag{21}$$

where $\underline{q}$, $\underline{\dot{q}}$, $\underline{\ddot{q}}$ are 6×1 vectors of body-segmental displacements, velocities, and accelerations; $Q(q)$ is the 6×1 Jacobian of the constrained dynamical system; $\underline{\lambda}$ is the vector of constraint forces acting on the skeleton (In our model, it contains only the force exerted at the tibiofemoral joint.); $\underline{F}^{MT}$ is an 8×1 vector of musculotendon actuator forces; u_i is the input excitation given to the ith muscle in the model; a_i is the level of activation in the ith muscle; τ_{rise} and τ_{fall} are the rise and decay times for muscle activation, respectively; x_k, y_k, and ϕ_k are the three generalized coordinates describing motion of the unconstained knee model (Fig. 1); M(q) is a 6×8 moment-arm matrix formed by computing the perpendicular distance between each musculotendon actuator and the joint it spans; A(q) is the 6×6 system mass matrix; $C(q)$ is a 6×1 vector containing only gravitational terms; $B(q)\,\underline{\dot{q}}^2$ is a 6×1 vector describing both Coriolis and centrifugal effects, where $\underline{\dot{q}}^2$ represents $\dot{q}_i^2$ for $i=1,\ 6$; D is a 6×6 matrix which transforms joint forces and torques into segmental forces and torques; and $S(q,\ \dot{q})$ is a 6×1 vector of external joint torques applied to the body. $S(q,\ \dot{q})$ contains only the torque applied at the toes to keep the foot flat on the ground during the squat-to-stand movement. Note that Eqs. (18) and (19) together describe

the dynamics of the constrained skeletal system. Equation (18) describes the dynamics of the unconstrained, six degree-of-freedom skeleton, whereas Eq. (19) specifies the holonomic constraint which describes rotation and slipping of the femur on the tibia (see below).

3.2 Dynamics of constrained skeletal system

We used the constraint embedding method described by Kane (1961) to incorporate the holonomic constraint for knee motion (Eq. (19)) into the unconstrained dynamical equations of motion for the skeletal system (Eq. (18)). The Jacobian matrix for the constrained skeletal system, $Q(q)$, can be found using the holonomic constraint defined by Eq. (12). Thus,

$$Q(q)=[0\ 0\ g_2\ 0\ g_1\ 1] \tag{22}$$

By definition, the orthogonal complement of $Q(q)$ is a matrix $T(q)$ given by

$$T(q)\,Q(q)\,T=0 \tag{23}$$

where in our model $T(q)$ is a 5×6 matrix. If the equations of motion for the unconstrained skeletal system are premultiplied by T(q), Eq. (18) reduces to

$$T(q)A(q)\,\underline{\ddot{q}}=T(q)\,[B(q)\,\underline{\dot{q}}^2+C(q)+DM(q)\,\underline{F}^{MT}+S(q,\ \dot{q})] \tag{24}$$

Also, differentiating the holonomic constraint for knee motion (Eq. (19)) with respect to time gives an equation of the form

$$Q(q)\,\underline{\dot{q}}=-\frac{\partial Q(q)\,\dot{q}}{\partial q}\,\underline{\dot{q}} \tag{25}$$

Equations (24) and (25) represent the dynamical equations for the constrained skeletal system, and can be solved for the vector of body-segmental accelerations at any instant in time. Specifically, embedding the holonomic constraint (Eq. (25)) into the unconstained dynamical equations of motion (Eq. (26)), we get

$$\underline{\ddot{q}}=\begin{pmatrix}T(q)A(q)\\ Q(q)\end{pmatrix}^T \begin{pmatrix}T(q)\,[B(q)\,\underline{\dot{q}}^2+C(q)+DM(q)\,\underline{F}^{MT}+S(q,\ \dot{q})]\\ -\dfrac{\partial Q(q)\,\dot{q}}{\partial q}\,\underline{\dot{q}}\end{pmatrix} \tag{26}$$

Equation (26) describes the dynamics of the constrained skeletal system. Note that $\underline{q}$ is a 6×1 vector comprising the generalized coordinates θ^f, θ_a, θ_h, x_k, y_k, and ϕ_k, where θ_f, θ_a, and θ_h represent the angle of the foot, ankle, and hip, respectively. To solve Eq. (26) for $\underline{\ddot{q}}$, the matrix $T(q)$ must be found. The unconstrained skeletal linkage has six degrees of freedom. However, with one holonomic constraint, the skeleton possesses five degrees of freedom, and can be described by the independent coordinates θ_f, θ_a, θ_h, x_k, y_k, and ϕ_k. Here, y_k is arbitrarily chosen to be the dependent coordinate. Using Eq. (12), the independent and dependent coordinates can be separated as follows:

$$\dot{y}_k+[g_1\ \ g_2]\begin{bmatrix}\dot{x}_k\\ \dot{\phi}_k\end{bmatrix}=0 \tag{27}$$

In this case, the matrix T(q) has the form (Kane, 1961):

$$T(q)=\begin{bmatrix}1 & & & & & \\ 0 & 0 & -g_2 & 0 & -g_1 & \end{bmatrix}^T \tag{28}$$

With the 5×6 matrix $T(q)$ defined by Eq. (28), the dynamical equations of motion for the constrained skeletal system (Eq. (26)) can be integrated forwards in time to compute the required body-segmental displacements, velocities, and accelerations.

3.3 Musculotendon properties and musculoskeletal geometry

Parameters defining nominal muscle properties (i. e., maximum isometric strength and the corresponding pennation angle and length of the muscle fiber) for each of the eight musculotendinous units in the model were estimated from data reported in Wichiewicz et al. (1983). The linear stress-strain curve for tendon was specified using values of elastic moduli obtained from Woo et al. (1982), while cross-sectional areas were chosen to give a reasonable strain in tendon at muscle's peak isometric force. Since no experimental data exist for tendon rest length, we adjusted this parameter for each actuator in the model until the total isometric, active torque about each

joint peaked at a joint angle corresponding to in vivo measurements of joint torque. The musculoskeletal geometry of the model (musculotendon origin and insertion sites) was defined on the basis of data reported in Brand et al. (1982). Finally, body-segmental parameters (i. e., segment mass and length, moment of inertia, and location of the center of mass of each segment) were scaled according to a 185 cm, 70 kg adult male using nominal data reported in Winter (1987).

4. Optimal Control Modeling

For rising from a squatting position, we chose to minimize the integral of normalized muscle stress summed over all the muscles in the model and integrated over the duration of the activity:

$$J=\min\int_0^{t_f}\sum_{i=1}^{8}\left(F_i^{MT}\Big/F_i^{\max}\right)^2 dt \tag{29}$$

where F_i^M is the force in the ith musculotendon actuator and F_i^{ma} is its maximum isometric strength. The constraints which govern the solution to the optimal control problem are the equations of motion for the constrained dynamical system (Eqs. (20), (21), and (26)), a set of inequality constraints which bound the magnitude of each muscle excitation signal to lie between zero (no excitation) and one (full excitation)

$$0\le u_i\le 1 \quad i=1,\ 8 \tag{30}$$

a set of terminal equality constraints that specify the position of the body segments at the final time, t_f,

$$q_i|_{t_f}=q_{if};\ i=1,\ 6 \tag{31}$$

and a terminal equality constraint that defines static equilibrium of the body at standing,

$$F_V(q,\ \dot{q},\ \ddot{q})|_{t_f}=\sum_{i=1}^{4}m_i g \tag{32}$$

Here $\underline{q}$ is the 6×1 vector of generalized coordinates comprising θ_f, θ_a, θ_h, x_k, y_k, and ϕ_k, m_i is the mass of the *ith* segment, g is the gravitational acceleration constant, F_V is the vertical ground force, and $|_{t_f}$ indicates that each quantity is evaluated at the final time. Thus, the optimal control problem is to minimize Eq. (29) subject to the given initial conditions (see below), the dynamical equations of motion (Eqs. (20), (21), and (26)), a set of path constraints (Eq. (30)), and a set of terminal constraints (Eqs. (31)-(32)). The optimal control problem, as formulated here, is a fixed final- time problem with $t_f=1$ sec.

4.1 Optimization of initial states

At time $t=0$, the model is in a static, squatting position with prespecified body-segmental angles and zero velocities. Thus, muscles exert torques about the ankle, knee, and hip to maintain the body in static equilibrium. However, with eight musculotendon actuators, there is an infinite combination of forces that will generate the required joint torques. To determine the initial muscle forces in the model as well as the location of the tibiofemoral contact force, we solved a static optimization problem by minimizing the sum of the squares of all muscle stresses:

$$J=\sum_{i=0}^{8}\left(F_i^{MT}\Big/F_i^{\max}\right)^2 \tag{33}$$

subject to six linear equality constraints (i. e., zero acceleration of all the body segments) and eight linear inequality constraints which constrain the magnitude of each muscle force to lie within a region defined by muscle's force-length property (see Garner, 1992 for details). Subsequent to computing muscle forces, Eq. (20) was used (with $\dot{\underline{F}}^{MT}=0$) to iteratively solve for the corresponding muscle activations.

4.2 Computation of optimal controls

We computed the optimal control solution using a computational algorithm which converts the optimal control problem into a parameter optimization problem. By specifying the neural excitation (control) histories for all the muscles at discrete intervals of time (nodes), values of neural excitation at each of these nodes form a set of unknown variables in the resulting parameter optimization problem. For the purpose of integrating the dynamical equations of motion, the continuous excitation history for each muscle was

then reconstructed by linearly interpolating between the control nodes. With arbitrary initial guesses for the control histories u, each iteration of the algorithm begins with a forward integration of the dynamical equations of motion (Eqs. (20), (21), and (26)) to compute the values of the performance index (Eqs. (29)) and the terminal constraints (equations (31)-(32)). First derivatives of each of these quantities with respect to the control nodes are then calculated numerically using forward differences. This requires multiple forward integrations of the dynamical equations of motion, one for each perturbation of the control nodes. Finally, values of the performance index, the constraints, and their derivatives are input into a standard nonlinear programming routine to obtain improved estimates of the values of the control nodes (see Pandy et al., 1990 for details).

5. Results and Discussion

Because the optimal control solution produces the complete time histories of all body motions, ground reaction forces, and muscle activation patterns, the response of the model can be quantitatively compared with measurements of the same variables obtained from subjects performing the same activity as the model. In a previous study, we recorded kinematic (video), force-plate, and EMG data as four, young, healthy, adult males stood up from a static squatting position (age 27 ±5 yr, height 180±5 cm, and body mass 75±5 kg, Garner, 1992; Pandy et al., 1993). To see whether our optimal control model could reproduce the major features of rising from a static squatting position, we compared the vertical ground reaction force predicted by the model with those generated by our subjects (see Fig. 3). In general, there was good agreement between model and experiment. Both the model and the subjects generated peak vertical ground forces on the order of body weight (compare heavy and light solid lines). We also found qualitative agreement between the predicted muscle excitations and measured EMG for many of the muscles in the lower extremity (not shown; Pandy et al., 1993).

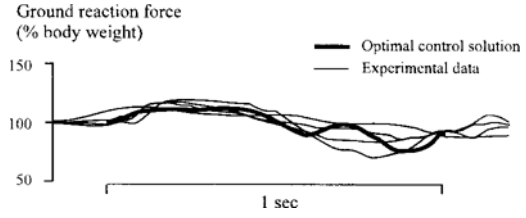

Fig. 3 Vertical ground reaction forces generated by the model (heavy solid line) and subjects (light solid lines) for rising from a static squatting position. The ground reaction force for the model was obtained by solving an optimal control problem which minimized the sum of all muscle stresses squared (see text for details). Notice that peak forces generated by the model and the subjects are near body weight.

In general, our two degree-of-freedom, dynamic model of the knee joint matched the observed sagittal-plane behavior of the knee. This conclusion is based on a comparison of the predicted location of the tibiofemoral contact point and the moment arms computed about the knee with experimental data reported in the literature (e. g. , Nisell, 1985). For example, Fig. 4 shows the variation in the location of the tibiofemoral contact force as a function of knee flexion angle as the model stood up from a static

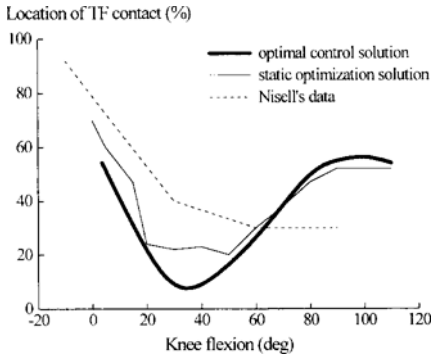

Fig. 4 Location of the tibiofemoral contact point obtained by solving a static optimization problem (light solid line) and an optimal control problem (heavy solid line) for rising from a static squatting position. The dashed line represents the location of the tibiofemoral contact force measured from cadaver experiments (Nisell, 1985). Note that 100% represents the anterior border of the tibial plateau.

squat (heavy solid line). To determine the effects of musculotendon and muscle activation dynamics on model response, we also solved a static optimization problem to find the muscle forces and the location of the tibiofemoral contact force using the body- segmental displacements obtained from a solution of the optimal control problem (Fig. 4, light solid line). In general, the location of the tibiofemoral contact force found using static optimization was similar to that obtained by solving the optimal control problem (compare solid lines in Fig. 4). Furthermore, these results agree well with measurements obtained from cadaver experiments (Fig. 4, dashed line; Nisell, 1985).

We also used the static optimization and optimal control solutions to compute the moment arm

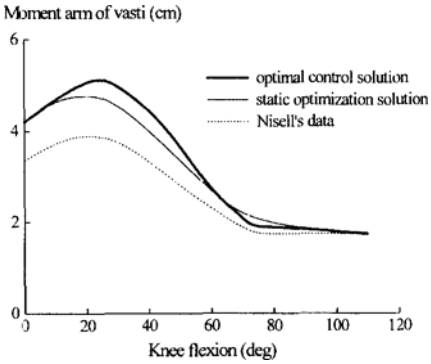

Fig. 5 Moment arm of vasti at the knee plotted against knee flexion angle. The moment arm found by solving a static optimization problem (light solid line) and an optimal control problem (heavy solid line) for rising from a static squat are nearly the same. The static optimization problem was solved for all the lower- extremity muscle forces as well as the location of the tibiofemoral contact force with the body placed in several positions and held in static equilibrium. The dashed line represents the moment arm of vasti computed by Yamaguchi and Zajac (1989) using Nisell's (1985) experimental data for the location of the tibiofemoral contact point and assuming that the femur rolls on the tibia. The light solid line represents the moment arm of vasti computed using our planar knee model together with Nisell's measured location of the tibiofemoral contact point (see text for discussion).

of vasti about the knee. The difference in the moment arm computed by these two methods was almost imperceptible (Fig. 5, compare light and heavy solid lines). These results, however, were significantly different from that reported by Yamaguchi and Zajac (1989) who based their moment arm calculation on Nisell's (1985) experimental data for the location of the tibiofemoral contact point (compare light and heavy solid lines with dashed line). To see whether this difference in the computed moment arm of vasti was due to a difference in the location of the tibiofemoral contact point predicted by our model and that used by Yamaguchi and Zajac (difference between the dashed and heavy solid lines in Fig. 4), we recomputed the moment arm for vasti in our model using Nisell's experimental data for the location of the tibiofemoral contact point (light solid line in Fig. 5). We found little difference in the computed moment arm for vasti when Nisell's data for the location of the tibiofemoral contact point were used in our model (Fig. 5, compare dashed and heavy solid lines with light solid line). The reason the moment arm for vasti reported by Yamaguchi and Zajac is so different from that predicted by our model (as much as 2 cm at 20-30 degrees of knee flexion) is due to Yamaguchi and Zajac's assumption that the femur rolls on the tibia. This condition has a significant affect on the moment arm computed at the knee since it means that the moment arm is calculated under the assumption that the instantaneous axis of rotation is at the point of tibiofemoral contact (Yamaguchi and Zajac, 1989). Because our model assumes that the femur rotates and slips on the tibia, the instantaneous axis of rotation lies at the center of curvature of the femoral condyles, which alters the moment arm for vasti significantly.

Using the muscle forces obtained from the static optimization and optimal control solutions, we also calculated the total contact force at the tibiofemoral joint during rising from a static squat (Fig. 6). The tibiofemoral contact force obtained by static optimization was much lower than that predicted by the optimal control solution (compare magnitude of forces in Fig. 6(a)

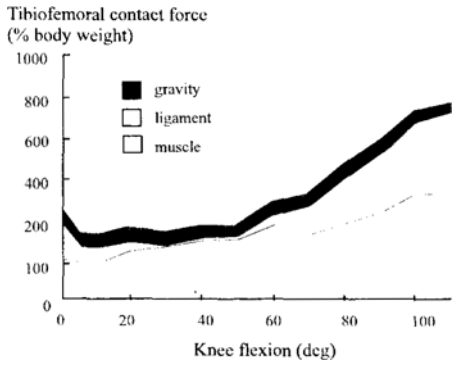

(a) Static model

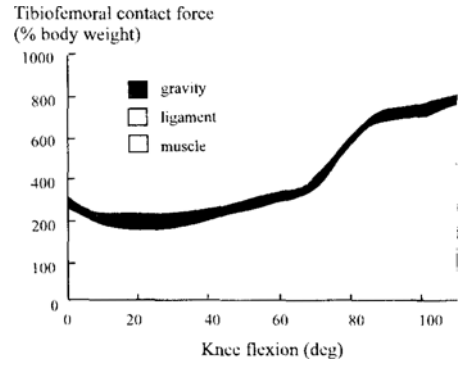

(b) Dynamic model

Fig. 6 Tibiofemoral contact force found by solving a static optimization problem (a) and an optimal control problem (b) for rising from a squatting position. The total tibiofemoral load is the sum of the contributions made by gravity and inertia (heavy shaded region), ligament (unshaded region), and muscle (light shaded region). Notice that muscle's contribution dominates the total force exerted at the tibiofemoral joint. Notice also that the optimal control solution yields much larger tibiofemoral loads (8 times body weight) than those predicted using static optimization (5 times body weight).

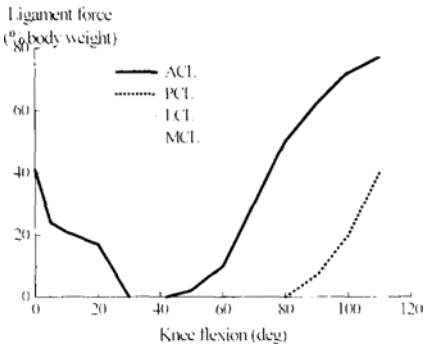

(a) Static model

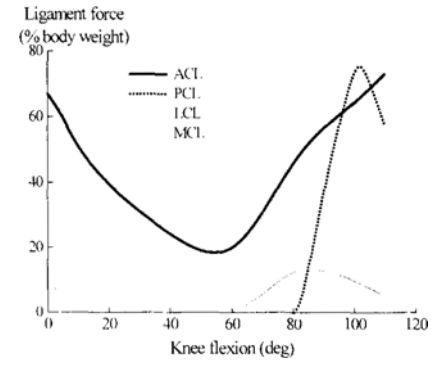

(b) Dynamic model

Fig. 7 Forces exerted by the anterior-cruciate ligament (ACL), posterior-cruciate ligament (PCL), lateral-collateral ligament (LCL), and medial-collateral ligament (MCL) in our model found by solving a static optimization problem (a) and an optimal control problem (b) for rising from a squatting position. In general, the ACL takes a large portion of the total load shared by all the ligaments in the model.

- (b)). Peak contact force at the tibiofemoral joint computed using static optimization was about 5 times body weight (Fig. 6(a)), whereas the optimal control solution predicted loads as high as 8 times body weight (Fig. 6(b)). In both cases, however, peak forces at the tibiofemoral joint occurred with the body in the initial deep-squatting position. We also computed the contributions from gravity, inertia, ligament, and muscle to the total tibiofemoral contact force (Fig. 6). Not surprisingly, muscle dominates the total load exerted at the tibiofemoral joint (Fig. 6, compare light shaded regions with total). The contribution from all the ligaments, however, was not insignificant. Both the static optimization and optimal control solutions gave ligament forces that were about 30 percent of the total contact force (Fig. 6, compare light unshaded regions with total), whereas gravity and inertia contributed less than 10 percent to the total load (Fig. 6, compare heavy shaded regions with total). The static optimization and optimal control solutions

produced significantly different tibiofemoral contact loads for rising from a static squat because the muscle forces predicted by these two methods were very different. Any difference in the muscle forces predicted by static optimization and optimal control is a measure of the effect that musculotendon dynamics has on the time history of muscle force. Although the tibiofemoral contact force predicted by our optimal control model is somewhat higher than that reported by others (Cheng, 1988; Collins and O'Connor, 1991; Fijan, 1990), our calculation was based on the assumption that point contact exists between the femur and tibia in the sagittal plane. Because tibiofemoral contact usually occurs in both the medial and lateral sides of the joint, forces transmitted at the knee in vivo are likely to be lower than those predicted by our planar model. Since the optimal control solution for standing up accounts for musculotendon dynamics and muscle excitation-contraction dynamics, we believe that the muscle, ligament, and tibiofemoral contact forces predicted by our model are more indicative of the actual loads transmitted at the knee during movement.

Finally, the forces exerted by each of the cruciate and collateral ligaments during rising from a static squat are shown in Fig. 7. We found general agreement between the ligament forces calculated using static optimization and our optimal control model. The anterior-cruciate ligament (ACL) took most of the load exerted by all the ligaments, with peak forces being as high as 80 percent body weight (Fig. 7, ACL). The optimal control solution predicted peak forces in the posterior-cruciate ligament (PCL) which were comparable to those exerted by the ACL, but the PCL took most of its load only when knee flexion exceeded 90 degrees (Fig. 7 (b), compare ACL and PCL in the squatting position). The collateral ligaments exerted forces that were significantly lower than those in either the ACL or the PCL, a result which we suspect is an artifact of modeling the knee in the sagittal plane.

References

Abdel-Rahman, E. M. and Hefzy, M. S., 1993, "Two dimensional dynamic model of the tibiofemoral joint," *J. Biomech. Engng.*, Vol. 115, pp. 350~356.

Alexander, R. McN. and Vernon, A., 1975, "The dimensions of knee and ankle muscles and the forces they exert," *J. Hum. Mvmt. Stud.* Vol. 1, pp. 115~123.

Andriacchi, T. P., Mikosz, R. P., Hampton, S. J., and Galante, J. O., 1983, "Model studies of the stiffness characteristics of the human knee joint," *J. Biomechanics,* Vol. 16, pp. 23~29.

Blankevoort, L., 1991, "Passive motion characteristics of the human knee joint: Experimental and computer simulations," PhD thesis, Catholic University Nijmegen, The Netherlands.

Brand, R. A., Crowninshield, R. D., Wittstock, C. E., Pederson, D. R., Clark, C. R., and van Krieken, F. M., 1982, "A model for lower extremity muscular anatomy," *Biomech. Engng.*, Vol. 104, pp. 304~310.

Cheng, D. L., 1988, "A mathematical model for predicting bony contact forces at the knee during human gait," Ph. D. thesis, Dept. of Civil and Environmental Engineering, University of Iowa.

Collins, J. and O'Connor, J., 1991, "Muscle-ligament interactions at the knee during walking," *Proc. Instn. Mech. Engrs.* Part H, Vol. 205, pp. 11~18.

Fijan, R. S., 1990, "A three-dimensional mathematical model of the human knee joint," Ph. D. thesis, Mechanical Engineering Dept., M. I. T.

Garg, A. and Walker, P. S., 1990, "Prediction of total knee motion using a three-dimensional computer-graphic model," *J. Biomechanics,* Vol. 23, pp. 45~50

Garner, B. A., 1992, "A dynamic musculoskeletal computer model for rising from a squatting or sitting position," Masters thesis, Dept. of Mech. Eng., University of Texas at Austin, Austin, Texas.

Kane, T. R., 1961, "Dynamics of nonholonomic systems," *J. of Applied Mechanics,* Vol. 28, pp. 574~578.

Mikosz, R. P., 1986, "Mathematical model for the study of forces in the human knee joint during locomotion," Ph. D. thesis, Dept. of Civil Eng., Mechanics, and Metallurgy, University of Illinois.

Moeinzadeh, M. H., Engin, A. E., and Akkas, N., 1983, "Two-dimensional dynamic modelling of human knee joint," *J. Biomechanics,* Vol. 16, pp. 253~264.

Morrison, J. B., 1970, "The mechanics of the knee joint in relation to normal walking," *J. Biomechanics,* Vol. 3, pp. 51~61

Nisell, R, 1985, "Mechanics of the knee," *Acta Orthop. Scand.* Supplementum 216, Vol. 56, pp. 1~42.

Pandy, M. G., Garner, B. A., and Anderson, F. C., 1993, "Optimal control of non-ballistic muscular movements: A performance criterion for rising from a chair," *J. Biomech. Engng.* Vol. 117, pp. 15~20.

Pandy, M. G., Anderson, F. C., and Hull, D. G., 1992, "A parameter optimization approach for the optimal control of large-scale musculoskeletal systems," *J. Biomech. Engng.* Vol. 114, pp. 450~460.

Pandy, M. G., Zajac, F. E., Sim, E., and Levine, W. S., 1990, "An optimal control model for maximum-height human jumping," *J. Biomechanics,* Vol. 23, pp. 1185~1198.

Wickiewicz, T. L., Roy, R. R., Powell, P. L., and Edgerton, V. R., 1983, "Muscle architecture of the human lower limb," *Clin. Orthop. Rel. Res.,* Vol. 179, pp. 275~283.

Wismans, J., Veldpaus, F., and Janssen, J., 1980, "A three-dimensional mathematical model of the knee joint," *J. Biomechanics,* Vol. 13, pp. 677~685

Wongchaisuwat, C., Hemami, H., and Buchner, H. J., 1984, "Control of sliding and rolling at natural joints," *J. Biomech. Engng.,* Vol. 106, pp. 368~375

Woo, S. L-Y and Gomez, M. A., Woo, Y., and Akeson, W. H., 1982, "Mechanical properties of tendons and ligaments. II. The relationships of immobilization and exercise on tissue remodeling," *Biorheology,* Vol. 19, pp. 397~408.

Winter, D. A., 1987, *The biomechanics and motor control of human gait,* Univ. Waterloo Press.

Yamaguchi, G. T. and Zajac, F. E., 1989, "A planar model of the knee joint to characterize the knee extensor mechanism," *J. Biomechanics,* Vol. 22, pp. 1~10.